www.sensorsportal.com

Sensors & Transducers

© 2014 by IFSA Publishing, S. L.

http://www.sensorsportal.com

Study of Dark Conductivity and Photoconductivity in Amorphous InAs Films Prepared at Different Working Pressure

[1] Yanping Yao, [2] Baoxue Bao, [2] Chunling Liu, [2] Xi Chang

[1] College of Information and Technology, Jilin Normal University, Siping 136000, China

[2] State Key Lab on High Power Laser Diodes, Changchun University of Science and Technology, Changchun 130022, China

[1] Tel.: +86-15804343721, fax: +86-0434-3292050

[1] E-mail: meyanping@163.com

Received: 21 March 2014 /Accepted: 31 July 2014 /Published: 31 August 2014

Abstract: Dark conductivity measurements and photoconductivity measurements were made on amorphous thin films of InAs prepared at different working pressure in the temperature range of 120–300 K. The experimental data suggest the conduction in the high-temperature region is found to be due to thermally assisted tunneling of the carriers in the localized states near the band edge, while that in low-temperature region takes place through variable range hopping of charge carriers in the localized states near the Fermi level. Various Mott's parameters have also been calculated for samples exhibiting variable range hopping conduction in the low temperature region. These results were analyzed in terms of the Davis–Mott model. The dependence of photoconductivity with light intensity shows that bimolecular recombination at high temperatures and monomolecular at low temperatures in amorphous InAs thin films. *Copyright © 2014 IFSA Publishing, S. L.*

Keywords: Amorphous, Mott's parameters, Conductivity, InAs, Working pressure.

1. Introduction

Crystal InAs has received considerable attention due to its application in high speed electronic devices, detectors and thermophotovoltaic devices. For the large lattice mismatch between InAs and substrate, it is hard to obtain crystal InAs films of high material quality. Amorphous InAs (*a*-InAs) is receiving much attention due to its potentiality for application in photoelectric devices and its low cost. Several workers have reported the electrical, optical and structural properties of *a*-InAs [1-2]. The application of the *a*-InAs material for the above devices is associated with the transport mechanism of charge carriers in this material. For the effective functioning of these devices the study and knowledge of transport mechanism is very important. However, hitherto no report in the literature about the transport mechanism of *a*-InAs films has been found. The photoconductivity is complex process and involves the absorption of light, the generation of excess carriers, and the transport and recombination mechanisms. The photoconductivity in *a*-InAs hasn't discussed in detail. In my present work, an attempt has been made to study photoconductivity and dark conductivity in *a*-InAs.

Mott and Davis showed that the plots of logσ_d (σ_d is the dark conductivity) versus $1/T$ (T is the temperature) in amorphous solids are found to consist of four distinct regions [3]. The four terms arise from four different conduction processes in this model of conduction. The dark conductivity is written as

$$\sigma_d = \sigma_0 \exp(-\frac{\Delta E_0}{kT}) + \sigma_1 \exp(-\frac{\Delta E_1}{kT}) \\ + \sigma_2 \exp(-\frac{W_2}{kT}) + \sigma_3 \exp(-\frac{T_0}{T^{1/4}}), \quad (1)$$

where σ_0-σ_3 is the pre-exponential factor, ΔE_0-ΔE_1 is the conduction activation energy, W_2 is the hopping energy, T_0 is the degree of disorder and k is the Boltzmann's constant respectively. The dark conductivity includes four conduction mechanism according to Eq. (1). In the first term on the right-hand side of Eq. (1), the conductivity is due to conduction in the extended states. In the second term on the right-hand side of Eq. (1), the contribution to the conductivity arises from thermally assisted tunneling of charge carriers in the localized states in band tails. The third term on the right-hand side of Eq. (1) represents the third contribution to conductivity in amorphous semiconductors which is analogous to impurity conduction in heavily doped semiconductors. This type of conduction mechanisms is Nearest-Neighbor Hopping (NNH). In the NNH hopping conduction, electron hops to the nearest neighbor empty site. This type of conduction also needs activation energy but this activation energy has much smaller value as compared to the energy required for thermally activated band conduction. The fourth term on the right-hand side of Eq. (1) is Variable Range Hopping (VRH), which the electrons hop between the levels that are close to Fermi level irrespective of their spatial distribution. In this type of hopping conduction, the hopping distance is not constant as in the nearest-neighbor hopping [4]. In this paper, we investigate the applicability of all four mechanisms to *a*-InAs films.

2. Experimental Method

Amorphous InAs films were deposited in a rf magnetron sputtering system in Ar ambient. A pure InAs (99.999 %) wafer with diameter of 50 mm was used as the sputtering target. Quartz glass was selected as substrate. These films were deposited at room temperature. Film growth was carried out in the growth ambient with working pressure ranging from 1 to 4 Pa and a rf power of 100 W. The distance between the target and substrate was fixed at 4 cm. Deposition time was 2 h.

The amorphous nature of the resulting glassy alloys was verified by D/MAX-IIB x-ray diffractometer (XRD) using Cu Kα radiation. Their chemical composition was determined by a scanning electron microscope (JSM-840) equipped with an energy-dispersive X-ray spectrometer (EDX) [5-6]. The dark conductivity was measured at various temperatures (120 to 300 K) with a pA m/dc-voltage source (with 10-14 A of sensitivity). I-V characteristics were found to be linear and symmetric up to 30 V in all the glasses studied. The present measurements were, however, made by applying only 6 V across the films. The low temperature was obtained by cooling the samples using liquid helium with a thermal regulation of 0.1 K. Before measurements, InAs films were coated with gold electrodes in the coplanar configuration which improved the contact characteristic between the Au and the substrate. The electrodes were 3 mm long and separated by 1 mm. The current–voltage (*I-V*) characteristics were analyzed and the conductivity was calculated from the formula:

$$\sigma = (I/V)(L/wd), \quad (2)$$

where L, w and d are the electrode length, electrode width and thin film thickness, respectively.

3. Results and Discussion

3.1. Structure and Composition

Fig. 1 gives a series of XRD patterns of samples grown under different working pressure. Thin films deposited at 2 Pa up to 4 Pa show amorphous structure. The results of EDAX quantitative calculation are shown in Table 1 at an error level of ± 1 at. %.

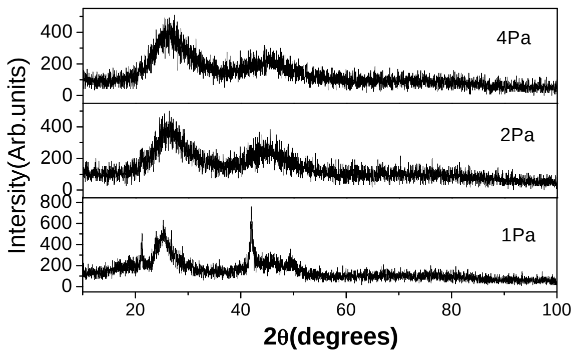

Fig. 1. XRD spectra of InAs thin films.

Table 1. EDX results of *a*-InAs films.

P_w (Pa)	In (at. %)	As (at. %)
2	53.7	46.3
3	52.14	47.86
4	52.47	47.53

The film composition is controlled by transport phenomena of sputtered atoms from the target to the substrate, and/or by substrate surface dynamics. During the transport process of the sputtered atoms, As is more rapidly thermalized by collisions with argon atoms, leading to In-rich in the InAs film as shown in Table 1.

3.2. Dark Conductivity and Conduction Mechanisms of *a*-InAs

Dark conductivity σ_d was the direct current (DC) conductivity of thin films under no light lumination condition. Fig. 2 shows the variation of dark conductivity current ($\log\sigma_d$) with applied temperature (1000/T) for *a*-InAs prepared at different working pressure.

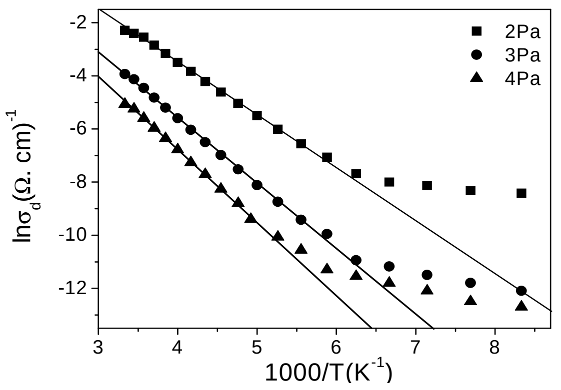

Fig. 2. Variation of dark current with applied temperature for *a*-InAs.

The $\ln\sigma_d$ versus 1000/T experimental curves generally show two distinct parts with different slopes. In the higher temperature range, the $\ln\sigma_d$ versus 1000/T curves exhibit a linear portion with larger slope. This shows that the activation type of conduction is dominating in the higher temperature range. In this temperature interval, the calculated values of activation energy and pre-exponential factor are given in Table 2.

It is suggested from Table 2 that the conduction is due to thermally assisted tunneling of charge carriers in the localized states in band tails and is expressed by the second term of the right-hand side of Eq. (1). It may, however, be mentioned that the activation energy alone does not provide any indication as to whether conduction takes place in the extended states above the mobility edge or by hopping in the localized states. This is because of the fact that both of these conduction mechanisms can occur simultaneously. The activation energy in the former case represents the energy difference between mobility edge and Fermi level, E_c-E_f or E_f-E_v [7-8]. In the latter case, it represents the sum of the energy separation between occupied localized state and the Fermi level, and the mobility activation energy for the hopping process between the localized states. In order to obtain a clear distinction between these two conduction mechanisms, Mott has suggested that the pre-exponential factor σ_1 of Eq. (1) for conduction in the localized states should be about 10^3 Ω^{-1}cm^{-1}, which is two to three orders smaller than for conduction in the extended states, and should become still smaller for conduction in the localized states near the Fermi level [9]. The magnitude of ΔE_1 and σ_1 in the present work indicate that the conduction is due to thermally assisted tunneling of charge carriers in the localized states present in the band tails. Table 2 shows the variation in pre-exponential factor, dc conductivity (σ_d) and activation energy (ΔE_1) with working pressure. The increase in the value of σ_1 with the increase of working pressure shows that the mobility of charge carriers in the trap states decreases. This is the main reason for the decrease in the conductivity of the samples and a increase in the ΔE_1.

Table 2. Electrical parameters for *a*-InAs films.

P_w (Pa)	σ *at* 300 K (Ω^{-1} cm^{-1})	σ_1 (Ω^{-1} cm^{-1})	ΔE_1 (eV)	σ_2 (Ω^{-1} cm^{-1})	ΔE_2 (eV)
2	1.01×10^{-1}	86.23	0.17	3.41×10^{-3}	0.03
3	1.97×10^{-2}	90.51	0.22	5.85×10^{-4}	0.04
4	5.29×10^{-3}	144.42	0.26	3.84×10^{-4}	0.05

At low temperature, the slope of straight line decreases but another straight line can be fitted in this temperature range having lower activation energy as compared to the first case. The activation energy for conduction (ΔE_2) and pre-exponential factor (σ_2) calculated from Eq. (1) are shown in Table 2. The pre-exponential factor σ_2 is about 10^{-3} Ω^{-1}cm^{-1} or smaller. The magnitude of ΔE_2 and σ_2 in the present work indicate that electrical conductivity corresponds to variable range hopping of localized states at E_F. This variable range hopping mechanism is characterized by Mott's expression of the form [10-13]:

$$\sigma = \sigma_0^{'} / T^{1/2} \exp\left(-T_0 / T^{1/4}\right), \tag{3}$$

where $\sigma_0^{'}$ and T_0 are given by the following expressions:

$$\sigma_0' = 3e^2 v_{ph}\left[N(E_F)/8\pi\alpha kT\right]^{1/2}, \tag{4}$$

$$T_0 = 16\alpha^3 / [k\ N(E_F)], \tag{5}$$

where v_{ph} is the Debye frequency (~10^{13} Hz), $N(E_F)$ the density of localized states at E_F, k is the

Boltzmann constant, T_0 is the degree of disorder, and a is the inverse localization length of the localized state.

From Eq. (3) we have,

$$\ln \sigma \sqrt{T} \propto T^{-1/4}, \tag{6}$$

Fig. 3 show $\ln \sigma \sqrt{T}$ vs. $T^{-1/4}$ plot for *a*-InAs. Thin films prepared at different working pressure. The straight line plot indicates that the dominant mechanism of conduction in the low temperature range is variable range hopping.

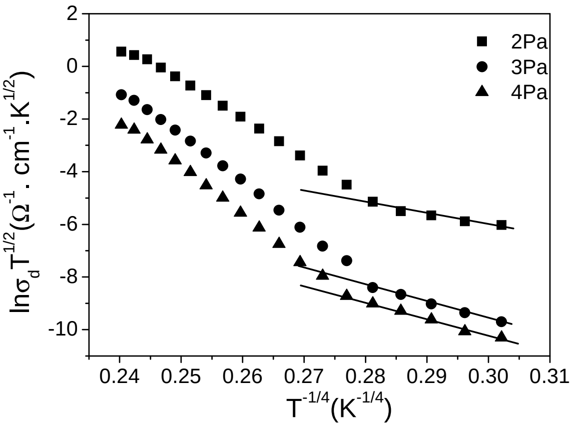

Fig. 3. The $\ln\sigma\sqrt{T}$ versus $T^{-1/4}$ curves for *a*-InAs thin films.

Simultaneous solution of Eqs. (4) and (5) yields

$$\alpha = 22.52\sigma_0' T_0^{1/2}, \tag{7}$$

and

$$N(E_F) = 2.12\times 10^9 \sigma_0'^3 T_0^{1/2}, \tag{8}$$

The hopping distance R and hopping energy W are given by

$$R = \{9/[8\pi\alpha kTN(E_F)]\}^{1/4}, \tag{9}$$

$$W = 3/[4\pi R^3 N(E_F)], \tag{10}$$

Various Mott parameters T_0, $N(E_F)$, α, R and W from Eqs. (4) - (10) are given in Table 3. It is found that the value of T_0 and R are increase with increasing working pressure. Since T_0 represent the degree of disorder, it follows that the amorphicity of the samples increases on increasing working pressure. It is also evident from Table 3 that the density of localized states $N(E_F)$ increases from 10^{25} eV^{-1} cm^{-3} to 10^{27} eV^{-1} cm^{-3}. The carrier concentration is 3.15×10^{18}cm^{-3} for the *a*-InAs film prepared at 2 Pa, whereas for *a*-InAs film prepared at 3 Pa and 4 Pa its values are 4.57×10^{18} cm^{-3} and 4.08×10^{18} cm^{-3} respectively. In the a-InAs film the change in carrier density is found to lead a large change in the value of $N(E_F)$. In the present case the lowest value $N(E_F)$ for the *a*-InAs film prepared at 2 Pa could be due to the lowest carrier concentration as compared to other two samples. We have calculated hopping energy (W). For the variable-range hopping conduction process, it is required that $\alpha R>1$ and $W>kT$ according to Mott and Davis. Thus the present measurement is in fair agreement with Mott condition of variable-range hopping conduction.

Table 3. Mott parameters for *a*-InAs prepared at different working pressure.

P_w (Pa)	T_0 (K)	σ'_0 (Ω^{-1}cm^{-1})	$N(E_F)$ (eV^{-1}cm^{-3})	α at 250 K	R at 250 K (cm)	W at 250 K (meV)	αR
2	4.20×10^6	2.33×10^4	5.49×10^{25}	1.07×10^9	3.23×10^{-9}	129.35	3.47
3	1.54×10^7	1.00×10^5	8.32×10^{27}	8.83×10^9	5.43×10^{-10}	179	4.80
4	1.73×10^7	9.20×10^4	6.87×10^{27}	8.62×10^9	5.74×10^{-10}	184.28	4.94

It is to further point out that an idea of the conduction process can also be obtained from the ratio of the average spacing between donors (r) with the effective Bohr radius (a^*) [4].

Here r is defined as:

$$r = [4\pi N_d/3]^{1/3}, \tag{11}$$

where N_d is the impurity carrier concentration density, a is the Bohr radius and have the value 0.53 Å. If $r/a^*>5$, the conduction is expected to be dominated by the nearest neighbor hopping between isolated donor levels, whereas for $2< r/a^* <5$, the variable range hopping conduction dominates. For $r/a^* <2$, in the high impurity concentration regime, the metallic conduction takes place because of overlapping of impurity and conduction bands. According to the carrier concentration in the a-InAs film, the r/a^* in the present case falls under second category, which indicates that VRH conduction process is expected to dominate.

3.4. Steady State Photoconductivity and Recombination Mechanism of *a*-InAs

To observe the effect of light at low temperatures, the whole sample is illuminated and the photocurrent is measured between two electrodes with the ohmic contacts. Photoconductivity, $\sigma_{ph,}$ is the additional photoconductivity of the excess number of photogenerated charge carriers under steady-state illumination. The photoconductivity has been computed by subtracting the dark conduction from the measured total conductivity of lumination, $\sigma_{p.}$ That's $\sigma_{ph}=\sigma_p$-σ_d. The temperature dependence of photoconductivity in *a*-InAs is plotted in Fig. 4. On the basis of the nature of slope, the temperature region is divided into two regions which are high temperature regions and lower temperature regions. This indicates that photoconductivity has two component.

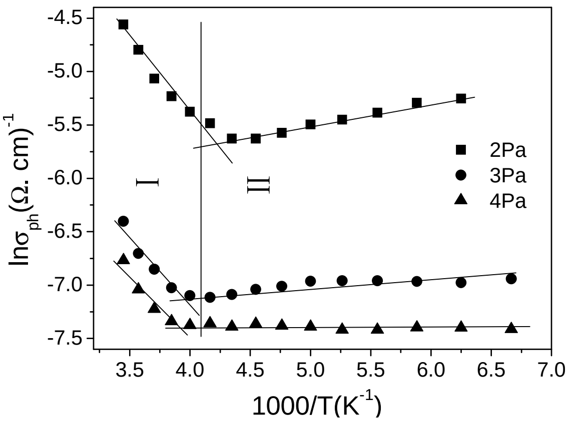

Fig. 4. Conductivity against the inverse temperature for *a*-InAs.

The steady state photoconductivity σ_{ph} is given by

$$\sigma_{ph} = eG\tau\mu\,, \tag{12}$$

where G, τ and μ are the generation rate of the photocarriers, combination time and photocarrier mobility, respectivily. The μ in amorphous InAs thin film is smaller than that of InAs crystal material. The lower μ shows lots of defects existing in *a*-InAs thin film and represents the hopping mobility when transport occurs in the tails tates. However μ in crystal material is the photocarrier mobility and transport occurs in the extended states. The dependence of τ on G already has gained by Wronski and Daniel as [14]:

$$\tau \propto G^{-(1-\gamma)}\ \sigma_{ph} \propto G^{\gamma}\,, \tag{13}$$

Simultaneous solution of Eqs. (12) and (13) yields:

$$\sigma_{ph} \propto G^{\gamma}\,, \tag{14}$$

where γ is the exponent, which determines the recombination mechanism. The value of γ = 0.5 indicates a bimolecular recombination type occurring through recombination centers (dangling bonds, for instance), where as γ=1.0 indicates a monomolecular recombination process in which the excess carriers recombine directly from the band tails [15].

When multiple reflections are neglected, G can be written as

$$G = \eta F(1-R)\left[1-\exp(-\alpha d)\right]/d\,, \tag{15}$$

where η is the quantum efficiency of the generation of photo carriers, F is the incident light intensity, R is the reflectivity, α is the absorption coefficient and d is the thickness of thin film respectively. Thereby, from the above discussion we can get

$$\sigma_{ph} \propto F^{\gamma}\,, \tag{16}$$

The dependence of photoconductivity with light intensity in *a*-InAs thin film is shown in Fig. 5 (a)-(b) respectively for 240 K and 170 K. The lnσ_{ph} versus ln$F$ curves are straight lines at the measuring temperatures. The value of γ is calculated from the slope of the lnσ_{ph} versus ln$F$.

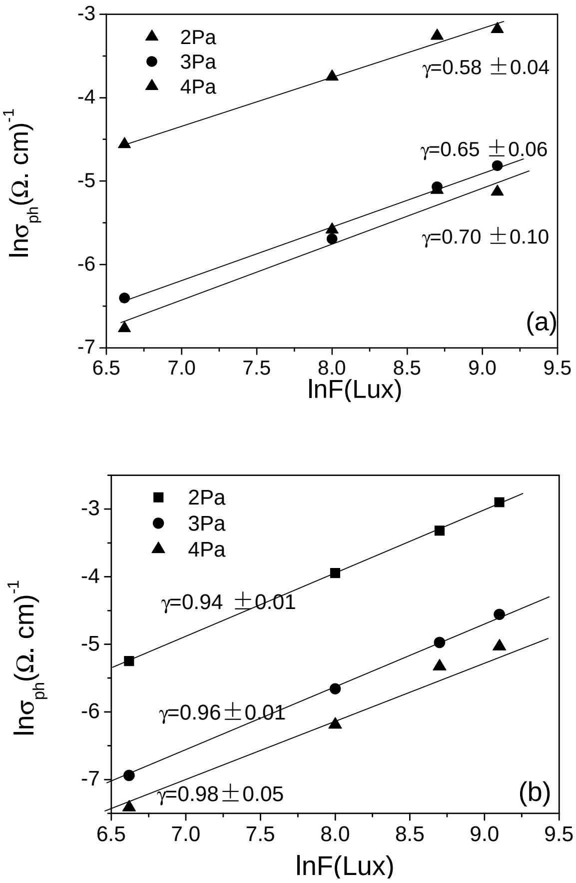

Fig. 5. The dependence of photoconductivity with light intensity in *a*-InAs thin film.

When temperatures increases, the mobility may not be yet large enough to allow the larger number of excess carriers to meet a recombination center although the carrier mobility increases with temperature. Under these conditions, a direct recombination process takes place between electrons and holes localized in the band tails, a bimolecular recombination [16]. In the present case as shown in Fig. 5 (a), the value of γ lies between 0.58 and 0.70 that can be considered as a case of bimolecular recombination.

At low temperatures, the demarcation levels for holes and electrons are expected to shift apart toward the band tails with temperature decreasing. By definition, all the states located between the demarcation levels act as recombination centers. Hence, at lower temperature we expect to have a larger density of recombination centers. This fact, combined with the reduced carrier mobility which is thermally activated in *a*-InAs, will favor a monomolecular-like recombination mechanism, yielding $\gamma \sim 1.0$, as indeed observed in Fig. 5 (b).

4. Conclusions

The *a*-InAs films were deposited at different working pressure using RF sputtering technique. To understand the electrical transport phenomena, the temperature dependence of DC conductivity for *a*-InAs films is studied over a temperature range of (120-300 K). On the basis of temperature dependence of conductivity, it is suggested that the conductivity arises from thermally assisted tunneling of charge carriers in the localized states in band tails in the high-temperature region, while in the low-temperature region the conduction takes place via variable range hopping in the localized states near the Fermi level. Various Mott's parameters such as density of states, degree of disorder, hopping distance, hopping energy are estimated. The value of T_0 and $N(E_F)$ were found to be increase with the increasing of working pressure. The steady state photoconductivity measurements at different temperatures indicate that the temperature region is divided into two regions. The intensity dependence of photoconductivity shows bimolecular recombination at high temperatures region and monomolecular at low temperatures region.

References

[1]. Driscoll C. M. H., Barthe J. R., Oberhofer M., *et al.*, Annealing procedures for commonly used radiothermoluminescent materials, *Radiation Protection Dosimetry*, Vol. 14, Issue 1, 1986, pp. 17-32.

[2]. Shevchik N. J., Tejeda J., Langer D. W., *et al.*, Similarities in the valence bands of amorphous and crystalline GeTe determined by X-ray photoemission, *Physical Review Letters*, Vol. 30, Issue 14, 1973, pp. 659.

[3]. Sharma A. K., Reddy P. J., Electrical properties of amorphous and crystalline InSb and InAs thin films, *Journal of Non-Crystalline Solids*, Vol. 41, Issue 1, 1980, pp. 13-30.

[4]. Burrafato G., Mancini N. A., Santagati S., *et al.*, Electrical properties of electron-gun-evaporated InAs thin films, *Thin Solid Films*, Vol. 121, Issue 4, 1984, pp. 291-301.

[5]. Di Sia, P, Magnetic Force as Source of Electron Attraction: A Classical Model and Applications, *Journal of Mechatronics*, Vol. 1, Issue 1, 2012, pp. 48-50.

[6]. Md. Ahasan Habib, Mahe Zabin, Jia Uddin A., An Approach to Wavelet Based Image Denoising, *Journal Comput. Intell. Electron. Syst.,* Vol. 1, 2012, pp. 144-148.

[7]. Khan M., Zulfequar M., Husain M., Electrical conduction mechanism in amorphous $Se_{80}In_{20-x}Pb_x$ films, Vol. 2, Issue 5, *Current Applied Physics*, 2002, pp. 401-406.

[8]. N. F. Mott, E. A. Davis, Electronic Processes in Non-Crystalline Materials, *Oxford University Press,* 1971.

[9]. Abdullaev G. B., Mekhtieva S. I., Aliev G. M., Effect of Oxygen on Some Electrical Properties of Selenium, *Physica Status Solidi (B)*, Vol. 11, Issue 2, 1965, pp. 891-898.

[10]. Davis E. A., Mott N. F., Conduction in non-crystalline systems V, Conductivity, optical absorption and photoconductivity in amorphous semiconductors, *Philosophical Magazine*, Vol. 22, Issue 179, 1970, pp. 0903-0922.

[11]. Khan M., Kumar S., Husain M., *et al.*, The effect of annealing on the electrical conduction of amorphous $Bi_{0.5}Se_{99.4}Zn_{0.1}$ thin films, *Materials Letters*, Vol. 62, Issue 10, 2008, pp. 1572-1574.

[12]. Marshall J. M., Carrier diffusion in amorphous semiconductors, *Reports on Progress in Physics*, Vol. 46, Issue 10, 1983, pp. 1235-1237.

[13]. Kushwaha N., Shukla R. K., Kumar S., *et al.*, Anomalous behaviour in dark conductivity and photoconductivity in a-$Se_{85}Te_{15-x}$ Pb_x thin films at low temperatures, *Materials Letters*, Vol. 60, Issue 27, 2006, pp. 3260-3264.

[14]. Wronski C. R., Daniel R. E., Photoconductivity, trapping, and re-combination in discharge-produced, hydrogenated amorphoussilicon, *Physical Review B*, Vol. 23, 1981, pp. 794.

[15]. Arene E., Baixeras J., Steady-state photoconductivity and recombination process in sputtered hydrogenated amorphous silicon, *Physical Review B*, Vol. 30, Issue 4, 1984, pp. 2016-2025.

[16]. Kushwaha N., Kushwaha V. S., Shukla R. K., *et al.*, Effect of lead additive on photoconductive properties of Se–Te chalcogenide films, *Journal of Non-crystalline Solids*, Vol. 351, Issue 43, 2005, pp. 3414-3420.

2014 Copyright ©, International Frequency Sensor Association (IFSA) Publishing, S. L. All rights reserved.
(http://www.sensorsportal.com)